Nonlinear Dyn (2013) 74:153–164
DOI 10.1007/s11071-013-0955-z

ORIGINAL PAPER

A new curved gradient deficient shell element of absolute nodal coordinate formulation for modeling thin shell structures

D. Yan · C. Liu · Q. Tian · K. Zhang · X.N. Liu · G.K. Hu

Received: 23 November 2012 / Accepted: 8 May 2013 / Published online: 30 May 2013
© Springer Science+Business Media Dordrecht 2013

Abstract A curved gradient deficient shell element for the Absolute Nodal Coordinate Formulation (ANCF) is proposed for modeling initially thin curved structures. Unlike the fully parameterized elements of ANCF, a full mapping of the gradient vectors between different configurations is not available for gradient deficient elements, therefore it is cumbersome to work in a rectangular coordinate system for an initially curved element. In this study, a curvilinear coordinate system is adopted as the undeformed Lagrangian coordinates, and the Green–Lagrange strain tensor with respect to the curvilinear frame is utilized to characterize the deformation energy of the shell element. As a result, the strain due to the initially curved element shape is eliminated naturally, and the element formulation is obtained in a concise mathematical form with a clear physical interpretation. For thin structures, the simplified formulations for the evaluation of elastic forces are also given. Moreover, an approach to deal with the on-surface slope discontinuity is also proposed for modeling general curved shell structures. Finally, the developed element of ANCF is validated by several numerical examples.

D. Yan · C. Liu · Q. Tian · K. Zhang · X.N. Liu (✉) · G.K. Hu
Key Laboratory of Dynamics and Control of Flight Vehicle, Ministry of Education, School of Aerospace Engineering, Beijing Institute of Technology, Beijing 100081, China
e-mail: liuxn@bit.edu.cn

Keywords Absolute nodal coordinate formulation (ANCF) · Gradient deficient element · Shell element · Slope discontinuity

1 Introduction

Absolute Nodal Coordinate Formulation (ANCF) proposed by Shabana [1] has been of a great interest for analyzing the dynamics of flexible multibody systems [2, 3]. For this non-incremental finite-element method, global position and its gradients are used as nodal Degrees of Freedom (DOFs) to define element's configuration. This method leads to an exact description of the motion of rigid body, and it also keeps the element mass matrix as constant. Therefore it has a great advantage for dynamic analysis of multibody systems especially subjected to large deformation and rotation.

A large number of elements of ANCF have been developed for modeling both beam and shell structures with various material constitutive models [4, 5]. According to the definition of the nodal gradient coordinates, the ANCF elements can be classified into two groups: the fully parameterized elements and the gradient deficient elements. For the fully parameterized elements, the position gradients with respect to all the coordinate lines are included, which can lead to a general description of element deformation including shear mode [6–9]. Although more element

deformation modes including the cross-section deformation can be taken into account, the fully parameterized elements suffer often from several locking problems known as curvature thickness locking, shear locking and Poisson's locking [10]. Several techniques have been proposed to circumvent the element locking problems [10]. On the other hand, gradient deficient elements are proposed for modeling thin flexible components such as cables, belts or membranes. For these elements, only an element's central axis or mid-surface is described by a reduced set of position gradients to characterize element configuration. The motion of a material point follows the Kirchhoff assumption and the shear deformation is usually excluded. For the gradient deficient element, a number of formulations have been proposed for beam [11–13] and plate structures [14, 15]. Gerstmayr and Irschik [12] made a geometrically exact correction on the existing beam formulations, by distinguishing the spatial and material measure of curvature used to calculate the bending strain. Dmitrochenko and Pogorelov [14] proposed several rectangular (48 DOFs or 36 DOFs) and triangular (27 DOFs) gradient deficient plate elements, where the formulations are similar with the degenerated continuum approach. Dufva and Shabana [15] proposed a rectangular gradient deficient thin plate element, and Green-Lagrange strain defined in a rectangular coordinate system is employed to evaluate the element elastic forces. Generally, gradient deficient elements show more computational efficiency for thin structures because of reduced DOFs, better convergence characteristics and elimination of high frequency oscillation due to the transverse gradient components [13, 15]. More recently, Sanborn et al. [25] observed that a membrane locking phenomenon caused by curve-induced distortion can happen for gradient deficient elements, and proposed a technique to eliminate it.

Many engineering thin structures possess initially curved shapes, thus curved beam or shell ANCF elements are expected in modeling these thin structures instead of straight elements. However, contributions to curved ANCF elements are relatively few in the literature. For the fully parameterized ANCF, a curved element can be achieved by using the isoparametric mapping technique. Along this way, Sugiyama and Suda [8] proposed a fully parameterized curved beam element, and Mikkola and Shabana [9] generalized plate element to shell element. Because a full mapping of gradient vectors between different configurations is not available, the generalization of gradient deficient elements to initially curved ones is not as straightforward as for the fully parameterized elements. A curved gradient deficient beam element is proposed by Sugiyama et al. [16], where the strain caused by the initial curvature is eliminated using one-dimensional Almansi strain. Liu et al. [17] extended the straight plate element of ANCF [14] to the cylindrical shell element. However, the formulation of a general irregular curved gradient deficient shell element has not been reported. Another problem in discretizing a general curved surface is the on-surface slope discontinuity, since a rectangular mesh with uniform element size can rarely be achieved. The problem of the slope discontinuity of ANCF has been discussed by many authors and different techniques have been proposed for both fully [18] or gradient deficiently [19, 20] parameterized elements, aiming at the out-surface type of discontinuities, i.e. sharp corners, T-sections, etc. The orthogonal transformation method given in [19] preserves the Kirchhoff assumption at the node where out-surface slope discontinuity takes place, its application is, however, limited to commutative rotations. For a general motion, Shabana [20] proposed a method by introducing an extra coordinate line, and as a result shear deformation is allowed at the slope discontinuities. Therefore, unlike the fully parameterized elements, a strict method for the out-surface discontinuities under a general motion is not available yet for the gradient deficient elements.

In this paper, based on Green–Lagrange strain tensor measured in a curvilinear coordinate system, a curved gradient deficient shell element is proposed with the purpose of modeling initially curved thin structures by using arbitrary mesh of irregular quadrilateral elements. In addition, an approach to deal with on-surface slope discontinuity is also proposed in order to assemble different irregular elements. The paper is organized as follows. In Sect. 2, a new curved thin shell element is developed, and the formulation of the element internal energy as well as its computationally efficient simplification is given. In Sect. 3, the problem of on-surface slope discontinuity is discussed. In Sect. 4, five numerical examples are provided to verify the performance of the proposed element. Finally, the main results of the work are concluded in Sect. 5.

2 Curved gradient deficient thin shell element of ANCF

In formulation of fully parameterized ANCF elements, it is always convenient to work in a rectangular coordinate system regardless of straight or initially curved configuration of the elements [8, 9]. Because there is a full mapping from a complex initial element configuration to a master element, the technique required is no more than an isoparametric solid element. This is not the case for a curved gradient deficient ANCF element, where a curvilinear coordinate system is more suitable to identify the initial configuration.

Different configurations of a shell element of ANCF are depicted in Fig. 1. In the initial reference configuration, the position of an arbitrary point on the mid-surface of the gradient deficient shell element can be parameterized by [15]

$$\mathbf{r}_{C0}(\xi^1,\xi^2)=\mathbf{S}(\xi^1,\xi^2)\mathbf{e}_0, \tag{1}$$

where $\mathbf{S}(\xi^1,\xi^2)$ is the shape function and $\mathbf{e}_0$ is the initial nodal DOFs, with $\xi^1,\xi^2\in[0,1]$ being the canonical interpolation parameters. It should be noted that the element adopting such shape function has 36 DOFs [15], where the second order derivatives of position vector are not included in the nodal DOFs. Therefore the continuity of slope vectors is not guaranteed at the element interface. However, the following developments are also suitable for the elements with other shape functions. Here and henceforth, a quantity with C or 0 appearing in the subscript or superscript represents that it belongs to the mid-surface or the initial configuration, respectively. Thus in this curved initial configuration, the position of a material point labeled with (ξ^1,ξ^2,ξ^3) is defined by

$$\mathbf{r}_0(\xi^1,\xi^2,\xi^3)=\mathbf{r}_{C0}(\xi^1,\xi^2)+\xi^3\mathbf{n}_0(\xi^1,\xi^2), \tag{2}$$

where $\mathbf{n}_0$ is the unit vector normal to the mid-surface. The element local coordinate system ξ^1–ξ^2–ξ^3 naturally constitutes a curvilinear Lagrange (material) coordinate system in which the strain should be measured. The covariant base vectors along the three curvilinear coordinate lines are defined by

$$\begin{aligned}\mathbf{G}_1&=\frac{\partial\mathbf{r}_0}{\partial\xi^1}=\frac{\partial\mathbf{r}_{C0}}{\partial\xi^1}+\xi^3\frac{\partial\mathbf{n}_0}{\partial\xi^1},\\ \mathbf{G}_2&=\frac{\partial\mathbf{r}_0}{\partial\xi^2}=\frac{\partial\mathbf{r}_{C0}}{\partial\xi^2}+\xi^3\frac{\partial\mathbf{n}_0}{\partial\xi^2},\\ \mathbf{G}_3&=\frac{\partial\mathbf{r}_0}{\partial\xi^3}=\mathbf{n}_0=\frac{\mathbf{G}_1\times\mathbf{G}_2}{|\mathbf{G}_1\times\mathbf{G}_2|}.\end{aligned} \tag{3}$$

Under the Euler–Kirchhoff assumption, the motion of the material point, i.e. the current configuration, can be characterized by replacing the nodal DOF vector in Eqs. (1) and (2) with the current vector $\mathbf{e}$, that is,

$$\mathbf{r}_C(\xi^1,\xi^2)=\mathbf{S}(\xi^1,\xi^2)\mathbf{e}, \tag{4}$$

$$\mathbf{r}(\xi^1,\xi^2,\xi^3)=\mathbf{r}_C(\xi^1,\xi^2)+\xi^3\mathbf{n}(\xi^1,\xi^2), \tag{5}$$

where $\mathbf{n}$ is the unit normal vector of the element mid-surface in the current configuration.

In analogy, the covariant base vectors along the material coordinate lines in the current configuration are given by

$$\begin{aligned}\mathbf{g}_1&=\frac{\partial\mathbf{r}}{\partial\xi^1}=\frac{\partial\mathbf{r}_C}{\partial\xi^1}+\xi^3\frac{\partial\mathbf{n}}{\partial\xi^1},\\ \mathbf{g}_2&=\frac{\partial\mathbf{r}}{\partial\xi^2}=\frac{\partial\mathbf{r}_C}{\partial\xi^2}+\xi^3\frac{\partial\mathbf{n}}{\partial\xi^2},\\ \mathbf{g}_3&=\frac{\partial\mathbf{r}}{\partial\xi^3}=\mathbf{n}=\frac{\mathbf{g}_1\times\mathbf{g}_2}{|\mathbf{g}_1\times\mathbf{g}_2|}.\end{aligned} \tag{6}$$

According to the non-linear continuum mechanics [21], the Green strain tensor defined in the reference curvilinear coordinate system can be written as

$$E_{IJ}=\frac{1}{2}(C_{IJ}-C^0_{IJ}), \tag{7}$$

where $C_{IJ}=\mathbf{g}_I\cdot\mathbf{g}_J$ is the Green deformation tensor and $C^0_{IJ}=\mathbf{G}_I\cdot\mathbf{G}_J$, with subscripts $I,J=1,2,3$. Actually, due to the assumed mode of motion, the strain tensor described by Eq. (7) is of locally planar state in the tangent plane of the curved surface, i.e. the components related to ξ^3-direction are zero. It should be noted that the Green strain tensor is defined within the curvilinear coordinate system with the non-orthonormal bases in Eq. (3), which is generally not ready to be correlated by a constitutive equation. To this end, an orthonormal nonholonomic coordinate frame is constructed point-wise, with three orthonormal base vectors $\mathbf{a}_i$ $(i=1,2,3)$ defined as

$$\mathbf{a}_1=\frac{\mathbf{G}_1}{|\mathbf{G}_1|},\qquad \mathbf{a}_3=\mathbf{n}_0,\qquad \mathbf{a}_2=\mathbf{a}_3\times\mathbf{a}_1. \tag{8}$$

The Green strain tensor is then regularized to this orthonormal frame by the following transformation:

$$\varepsilon_{ij}=\beta_i^I\beta_j^J E_{IJ}, \tag{9}$$

with subscripts $i,j=1,2,3$, where the Jacobian between the two frames is defined as [26]

$$\beta_i^I=\mathbf{a}_i\cdot\mathbf{G}^I, \tag{10}$$

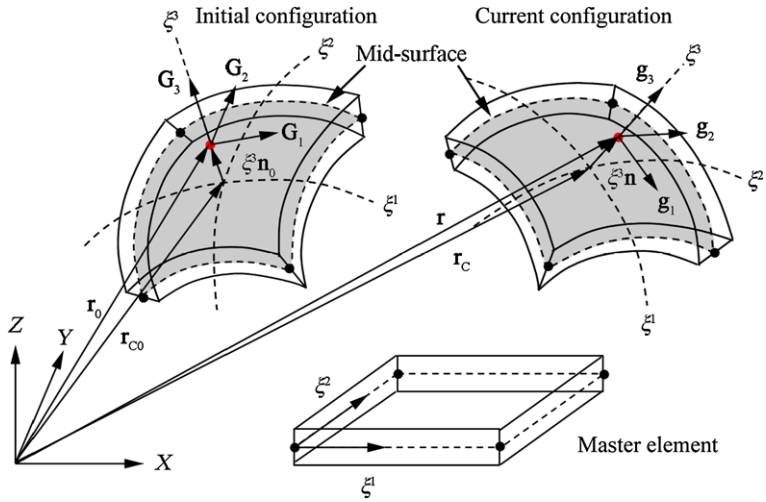

Fig. 1 Different configurations of a shell element of ANCF

and $\mathbf{G}^I$ is the contravariant base vector of the reference system defined by $\mathbf{G}^I \cdot \mathbf{G}_J = \delta^I_J$ with δ^I_J being the Kronecker Delta. For convenience, Eq. (9) can be expressed in a matrix form as

$$\begin{bmatrix} \varepsilon_{11} & \varepsilon_{12} \\ \varepsilon_{12} & \varepsilon_{22} \end{bmatrix} = \mathbf{T} \begin{bmatrix} E_{11} & E_{12} \\ E_{12} & E_{22} \end{bmatrix} \mathbf{T}^{\mathrm{T}}, \tag{11}$$

where

$$\mathbf{T} = \begin{bmatrix} \beta^1_1 & \beta^2_1 \\ \beta^1_2 & \beta^2_2 \end{bmatrix} \tag{12}$$

is the transformation matrix. In Eq. (11) only the nonzero entries, i.e. the membrane part of the strain component are kept. Adopting the linear elastic constitutive relation and expressing the strain tensor as the vector of Voigt form

$$\boldsymbol{\varepsilon} = [\varepsilon_{11} \quad \varepsilon_{22} \quad 2\varepsilon_{12}]^{\mathrm{T}}, \tag{13}$$

the deformation energy of the curved shell element can then be expressed as the following:

$$U = \frac{1}{2} \int_{V_0} \boldsymbol{\varepsilon}^{\mathrm{T}} \mathbf{D} \boldsymbol{\varepsilon} \, dV, \tag{14}$$

where

$$\mathbf{D} = \frac{E}{1-\nu^2} \begin{bmatrix} 1 & \nu & 0 \\ \nu & 1 & 0 \\ 0 & 0 & \frac{1-\nu}{2} \end{bmatrix} \tag{15}$$

is the constitutive matrix under the plane stress state with E and ν being the Young modulus and Poisson ratio, respectively.

The energy expression given by Eq. (14) is computational expensive since numerical integration over element volume is involved. For thin shell structures, simplification can be made by neglecting the quadratic terms of the ξ^3 coordinate in the thickness direction. With this simplification, the Green strain tensor in Eq. (7) can be separated into the membrane part E^l_{IJ} and the bending part E^b_{IJ} as

$$\tilde{E}_{IJ} = E^l_{IJ} + E^b_{IJ}, \tag{16}$$

$$E^l_{IJ} = \frac{1}{2}\left(\frac{\partial \mathbf{r}_{\mathrm{C}}}{\partial \xi^I} \cdot \frac{\partial \mathbf{r}_{\mathrm{C}}}{\partial \xi^J} - \frac{\partial \mathbf{r}_{\mathrm{C0}}}{\partial \xi^I} \cdot \frac{\partial \mathbf{r}_{\mathrm{C0}}}{\partial \xi^J} \right), \tag{17}$$

$$\begin{aligned} E^b_{IJ} &= \xi^3 \left(\frac{\partial \mathbf{r}_{\mathrm{C}}}{\partial \xi^I} \cdot \frac{\partial \mathbf{n}}{\partial \xi^J} - \frac{\partial \mathbf{r}_{\mathrm{C0}}}{\partial \xi^I} \cdot \frac{\partial \mathbf{n}_0}{\partial \xi^J} \right) \\ &= -\xi^3 \left(\frac{\partial^2 \mathbf{r}_{\mathrm{C}}}{\partial \xi^I \partial \xi^J} \cdot \mathbf{n} - \frac{\partial^2 \mathbf{r}_{\mathrm{C0}}}{\partial \xi^I \partial \xi^J} \cdot \mathbf{n}_0 \right) \\ &= -\xi^3 \left(K_{IJ} - K^0_{IJ} \right), \end{aligned} \tag{18}$$

where $K_{IJ} = \frac{\partial^2 \mathbf{r}_{\mathrm{C}}}{\partial \xi^I \partial \xi^J} \cdot \mathbf{n}$ and $K^0_{IJ} = \frac{\partial^2 \mathbf{r}_{\mathrm{C0}}}{\partial \xi^I \partial \xi^J} \cdot \mathbf{n}_0$ are the material measures of curvature [12, 15] of the deformed and initial curved mid-surface, respectively. In addition, the transformation defined in Eq. (9) can also be approximated to be ξ^3 irrelevant, i.e. the transformation corresponding to the point on mid-surface is used for all the points of the fiber with the same (ξ^1, ξ^2)

$$\mathbf{T}_{\mathrm{C}} = \begin{bmatrix} \beta^1_{1\mathrm{C}} & \beta^2_{1\mathrm{C}} \\ \beta^1_{2\mathrm{C}} & \beta^2_{2\mathrm{C}} \end{bmatrix}, \tag{19}$$

where $\beta^I_{i\mathrm{C}}$ represents β^I_i on the mid-surface. The corresponding regularized strains are expressed as

$$\varepsilon^l_{ij} = \beta^I_{i\mathrm{C}} \beta^J_{j\mathrm{C}} E^l_{IJ}, \tag{20}$$

$$\begin{aligned} \varepsilon^b_{ij} &= -\xi^3 \left(\beta^I_{i\mathrm{C}} \beta^J_{j\mathrm{C}} K_{IJ} - \beta^I_{i\mathrm{C}} \beta^J_{j\mathrm{C}} K^0_{IJ} \right) \\ &= -\xi^3 \left(\kappa_{ij} - \kappa^0_{ij} \right), \end{aligned} \tag{21}$$

where $\kappa_{ij} = \beta_{iC}^I \beta_{jC}^J K_{IJ}$ and $\kappa_{ij}^0 = \beta_{iC}^I \beta_{jC}^J K_{IJ}^0$ are, respectively, the current and initial material curvatures expressed in the orthonormal nonholonomic coordinate frame defined in Eq. (8).

Then the deformation energy of the element is simplified as

$$\tilde{U} = U^l + U^b, \tag{22}$$

where

$$U^l = \frac{h}{2}\int_0^1\int_0^1 \boldsymbol{\varepsilon}^{l\mathrm{T}}\mathbf{D}\boldsymbol{\varepsilon}^l |\mathbf{G}_{1\mathrm{C}} \times \mathbf{G}_{2\mathrm{C}}|\, d\xi^1\, d\xi^2, \tag{23}$$

$$U^b = \frac{h^3}{24}\int_0^1\int_0^1 \boldsymbol{\kappa}^{\mathrm{T}}\mathbf{D}\boldsymbol{\kappa} |\mathbf{G}_{1\mathrm{C}} \times \mathbf{G}_{2\mathrm{C}}|\, d\xi^1\, d\xi^2, \tag{24}$$

$$\boldsymbol{\varepsilon}^l = \begin{bmatrix}\varepsilon_{11}^l & \varepsilon_{22}^l & 2\varepsilon_{12}^l\end{bmatrix}^{\mathrm{T}}, \tag{25}$$

$$\boldsymbol{\kappa} = \begin{bmatrix}\kappa_{11} - \kappa_{11}^0 & \kappa_{22} - \kappa_{22}^0 & 2\left(\kappa_{12} - \kappa_{12}^0\right)\end{bmatrix}^{\mathrm{T}}, \tag{26}$$

and h is the thickness of the shell element. The elastic force vector and the mass matrix can be calculated by

$$\mathbf{Q} = \frac{\partial \tilde{U}}{\partial \mathbf{e}}, \tag{27}$$

$$\mathbf{M} = h\int_0^1\int_0^1 \rho \mathbf{S}^{\mathrm{T}}\mathbf{S} |\mathbf{G}_{1\mathrm{C}} \times \mathbf{G}_{2\mathrm{C}}|\, d\xi^1\, d\xi^2, \tag{28}$$

where ρ is the material density of the shell element.

The proposed formulas could be easily degenerated to the 2D curved gradient deficient thin beam element. In this situation, ξ^1–ξ^2 coordinate system is used and ξ^1 and ξ^2 are the central-axis direction and the thickness direction, respectively. The only non-zero regularized Green strain component is the axial one and can be expressed by

$$\varepsilon_{11} = \frac{1}{2\mathbf{G}_1 \cdot \mathbf{G}_1}[\mathbf{g}_1 \cdot \mathbf{g}_1 - \mathbf{G}_1 \cdot \mathbf{G}_1]. \tag{29}$$

The above strain can adopt a simplified formulation from which only numerical integration along the central axis is necessary in the elastic force evaluation. The simplified strain can also be separated as axial and bending part as

$$\begin{aligned}\varepsilon_{11} &\approx \varepsilon^l + \varepsilon^b \\ &= \frac{1}{2}\frac{1}{|\frac{\partial \mathbf{r}_{\mathrm{C0}}}{\partial \xi^1}|^2}\left(\frac{\partial \mathbf{r}_{\mathrm{C}}}{\partial \xi^1}\cdot\frac{\partial \mathbf{r}_{\mathrm{C}}}{\partial \xi^1} - \frac{\partial \mathbf{r}_{\mathrm{C0}}}{\partial \xi^1}\cdot\frac{\partial \mathbf{r}_{\mathrm{C0}}}{\partial \xi^1}\right) \\ &\quad - \frac{\xi^2}{|\frac{\partial \mathbf{r}_{\mathrm{C0}}}{\partial \xi^1}|^2}(\kappa - \kappa_0),\end{aligned} \tag{30}$$

where

$$\kappa = \frac{|\frac{\partial \mathbf{r}_{\mathrm{C}}}{\partial \xi^1} \times \frac{\partial^2 \mathbf{r}_{\mathrm{C}}}{\partial \xi^1 \partial \xi^1}|}{|\frac{\partial \mathbf{r}_{\mathrm{C}}}{\partial \xi^1}|} \tag{31}$$

is the material measure of curvature of the beam central axis in the current configuration, and κ_0 is the initial curvature. The strain measure in Eq. (30) agrees with the previous work in [16], where the strain is derived in a different way.

3 Element assembling with on-surface slope discontinuity

Despite of the advantages of ANCF element, an obvious deficiency is the complexity in dealing with the connectivity of the mesh, in particular, the discontinuities of the slope vectors between elements. There are a number of works devoted to the problem of slope discontinuity [18–20] for both fully and deficiently parameterized formulations, where efforts are made towards the out-surface slope discontinuity in the sharp corners, T-section etc. in the structure, while preserving the outstanding feature of constant mass matrix of ANCF.

Actually, even for meshing a smooth surface, the on-surface discontinuity of slope vector can take place constantly whenever irregular elements meet at a common node, or even the adjacent elements have different sizes, since it is preferable to interpolate the element geometry over a canonical master element. When a general curved surface is modeled, uniform rectangular mesh lines are seldom available, therefore at these on-surface slope discontinuities transformation is necessary before the element mass matrix and elastic force vector are assembled into the global ones. For the fully parameterized elements, the method given by [18] is a general one which can deal with on-surface or out-surface slope discontinuities. On the standing point of the 2D curvilinear local and global coordinate system on the surface, a constant transformation can be achieved towards the on-surface slope discontinuity for the gradient deficient elements.

As shown in Fig. 2, considering a smooth shell structure, at the node N on the mid-surface with the position vector of $\mathbf{r}_{\mathrm{C}}$, a pair of arbitrary coordinate lines (s, t) in the tangent plane can be chosen to define the gradient vectors, $\partial \mathbf{r}_{\mathrm{C}}/\partial s$ and $\partial \mathbf{r}_{\mathrm{C}}/\partial t$, which

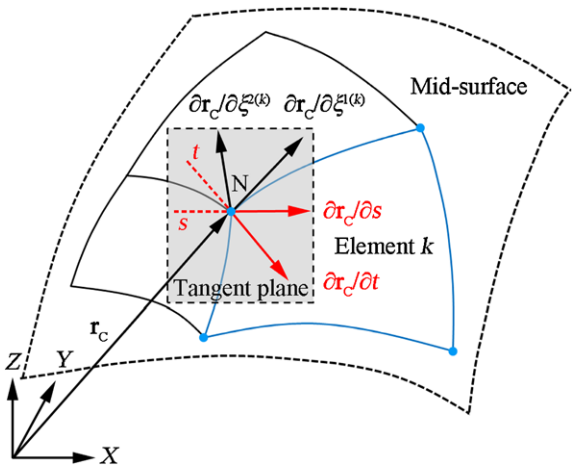

Fig. 2 Transformation between local nodal vector and global nodal vector

together with the position vector constitute the global nodal DOF vector

$$\mathbf{p} = [\mathbf{r}_C \quad \partial\mathbf{r}_C/\partial s \quad \partial\mathbf{r}_C/\partial t]^T. \tag{32}$$

In analogy with the concept used in the treatment of slope discontinuity for the fully parameterized element, the nodal vector $\mathbf{e}^{(k)}$ defined in the kth-element local coordinate system can be transformed from the global nodal vector through the following equation:

$$\mathbf{e}^{(k)} = \begin{bmatrix} \mathbf{r}_C \\ \frac{\partial \mathbf{r}_C}{\partial \xi^{1(k)}} \\ \frac{\partial \mathbf{r}_C}{\partial \xi^{2(k)}} \end{bmatrix} = \begin{bmatrix} \mathbf{I} & \mathbf{0} & \mathbf{0} \\ \mathbf{0} & \frac{\partial s}{\partial \xi^{1(k)}}\mathbf{I} & \frac{\partial t}{\partial \xi^{1(k)}}\mathbf{I} \\ \mathbf{0} & \frac{\partial s}{\partial \xi^{2(k)}}\mathbf{I} & \frac{\partial t}{\partial \xi^{2(k)}}\mathbf{I} \end{bmatrix} \begin{bmatrix} \mathbf{r}_C \\ \frac{\partial \mathbf{r}_C}{\partial s} \\ \frac{\partial \mathbf{r}_C}{\partial t} \end{bmatrix} = \mathbf{R}\mathbf{p}, \tag{33}$$

where the transformation matrix $\mathbf{R}$ remains constant during the deformation. Consequently all the important features of ANCF, particularly the property of the constant mass matrix, are kept. It should be mentioned that the transformation proposed here is restricted only to the on-surface one, i.e. the objective is to the assembling of an arbitrary irregular mesh of a smooth surface. The transformation of the deficient gradient vectors occurs in the tangent plane of a surface. It should be noted that Eq. (33) is essentially different with the constant orthogonal transformation given in [19] for gradient deficient elements. Actually, Eq. (33) has similar interpretation with the transformation developed in [18] for fully parameterized elements, except that the concept is extended here to the tangent plane of a curved surface for the deficient slope vectors.

In practice, the global coordinate lines across a node can be chosen arbitrarily in the tangent plane on the reference configuration, while for convenience they can be set to overlap with the local coordinates of a certain element k among the elements meet at the sharing node, i.e. $s = \xi^{1(k)}$ and $t = \xi^{2(k)}$. Hence the covariant bases of the global system are

$$\begin{aligned} \mathbf{F}_1 &\equiv \frac{\partial \mathbf{r}_{C0}}{\partial s} = \frac{\partial \mathbf{r}_{C0}}{\partial \xi^{1(k)}}, \\ \mathbf{F}_2 &\equiv \frac{\partial \mathbf{r}_{C0}}{\partial t} = \frac{\partial \mathbf{r}_{C0}}{\partial \xi^{2(k)}}. \end{aligned} \tag{34}$$

In another element l, the corresponding transformation items in Eq. (33) can be determined in a straightforward manner

$$\begin{aligned} \frac{\partial s}{\partial \xi^{1(l)}} &= \mathbf{F}^1 \cdot \frac{\partial \mathbf{r}_{C0}}{\partial \xi^{1(l)}}, & \frac{\partial s}{\partial \xi^{2(l)}} &= \mathbf{F}^1 \cdot \frac{\partial \mathbf{r}_{C0}}{\partial \xi^{2(l)}}, \\ \frac{\partial t}{\partial \xi^{1(l)}} &= \mathbf{F}^2 \cdot \frac{\partial \mathbf{r}_{C0}}{\partial \xi^{1(l)}}, & \frac{\partial t}{\partial \xi^{2(l)}} &= \mathbf{F}^2 \cdot \frac{\partial \mathbf{r}_{C0}}{\partial \xi^{2(l)}}, \end{aligned} \tag{35}$$

where $\mathbf{F}^1$ and $\mathbf{F}^2$ are the corresponding contravariant bases of the global system. The transformation matrix is prepared in the preprocessing stage and remains constant during the time marching of the structure motion. The validity of the proposed curved thin shell formulation with arbitrary quadrilateral mesh discretization will be verified by several case studies in the following section.

4 Numerical examples

In this section, five static and dynamic numerical examples are provided to validate the performance of the proposed gradient deficient curved thin shell element. The element shape function proposed by Dufva and Shabana [15] is adopted. All the results from statics analysis are validated by the commercial software ABAQUS. SI units are adopted for the parameters in the following examples.

4.1 Simple cantilever rectangular plate

A simple rectangular cantilever plate is subjected to two force components at the free end as shown in Fig. 3a. Previous works [15, 17] have used this test as a benchmark. The cantilever plate has dimensions of 0.5, 0.15, and 0.001, respectively for the length l, width w, and thickness h. The Young modulus and Poisson ratio are, respectively, 2.07×10^{11} and 0.3,

and the applied force P is 15. As shown in Fig. 3 calculations are performed with three different mesh patterns: Pattern 1 (regular rectangular mesh), Pattern 2 (rectangular mesh with different size) and Pattern 3 (mesh with irregular quadrilateral elements). a and b are the length and width of the regular element in Pattern 1, respectively. For the last two cases, on-surface discontinuities present at the sharing nodes. The deflections of the end tip for the three mesh patterns are shown in Table 1. It can be clearly observed that all the three mesh ways give convergent results, while the irregular mesh deviates slightly from the standard. This example confirms that the proposed method can deal with on-surface slope discontinuity caused by the assembling of the shell elements with irregular shapes. To shed a light on the performance of the element, eigenvalue analysis for a single element with typical configurations in accordance with the present rectangular plate and the following three static examples is performed, and the eigenvalues are listed in Table 2. It is observed that, for all cases, six and only six near-zero values corresponding to six rigid-body modes are observed.

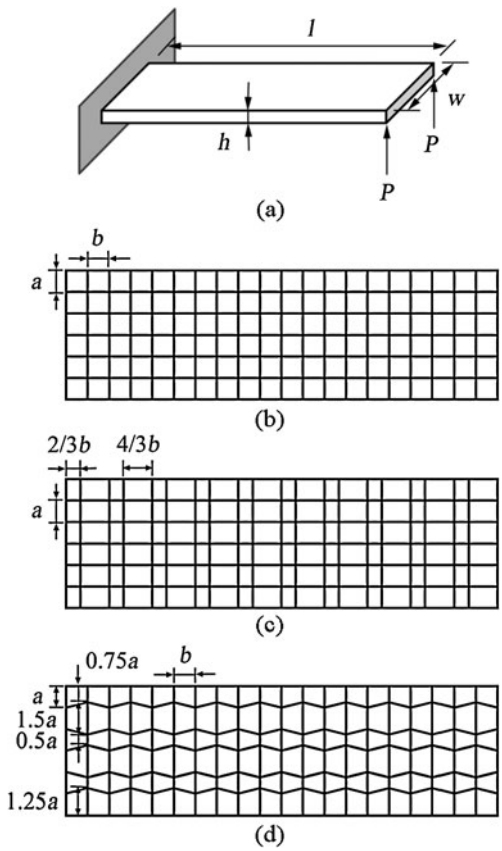

Fig. 3 (**a**) Rectangular cantilever plate with different meshes of (**b**) Pattern 1, (**c**) Pattern 2 and (**d**) Pattern 3

4.2 Slit annular plate under transverse line load

A clamped slit annular plate subjected to a distributed transverse load is shown in Fig. 4. This example is considered to test non-linear finite-element formulations for thin walled shell structures and has been extensively used by many investigators [22, 23]. The geometry and elastic material properties are listed as follows: Young modulus of 2.1×10^7, Poisson ratio of 0.0, outer radius of 10, inner radius of 6, thickness of 0.03 and a maximum distributed load q of 0.8. Tests are made with meshes 6 (circumferential direction) $\times$ 1 (radial direction), 18×3, 30×5, 60×10, and 90×15. Displacements of points A and B under distributed load $q = 0.8$ are shown in Fig. 5, as a function of the number of elements. It can be observed that the enough accuracy and converged result are produced up to 30×5 mesh. In Fig. 6, the results obtained by 90×15 mesh are compared with the S4R element in ABAQUS, where good agreement can be found. The deformed configuration under load $q = 0.8$ with 60×10 mesh is plotted in Fig. 7.

4.3 Hemispherical shell with 18° hole

This test is a classical double-curved shell problem commonly used to assess the element's ability to reproduce a correct membrane and bending state

Table 1 Comparison of the deflections of the end tip for the three mesh patterns

Element type	Mesh size	Mesh pattern	Deflection of the end tip
Curved shell element of ANCF	20×6	1	0.2866
Curved shell element of ANCF	20×6	2	0.2867
Curved shell element of ANCF	20×6	3	0.2882
S4R element in ABAQUS	20×6	1	0.2866

Table 2 Eigenvalues of one element with the configurations conforming with the four static examples: 1 rectangular plate, 2 slit annular plate, 3 hemispherical shell with 18° hole and 4 hemispherical shell without hole

Number	1	2	3	4	5	6	7	...	36
Example 1	6.00e–12	2.21e–9	2.21e–9	1.22e–8	1.22e–8	1.67e–7	5.13	...	9.20e+8
Example 2	1.73e–11	6.25e–11	9.76e–11	1.64e–10	1.64e–10	2.33e–10	7.03	...	1.23e+7
Example 3	3.27e–10	3.27e–10	4.46e–10	4.46e–10	1.90e–9	3.07e–9	1.64e+3	...	6.69e+7
Example 4	5.81e–11	1.98e–10	3.78e–10	5.91e–10	5.91e–10	6.34e–10	2.19e+2	...	1.44e+7

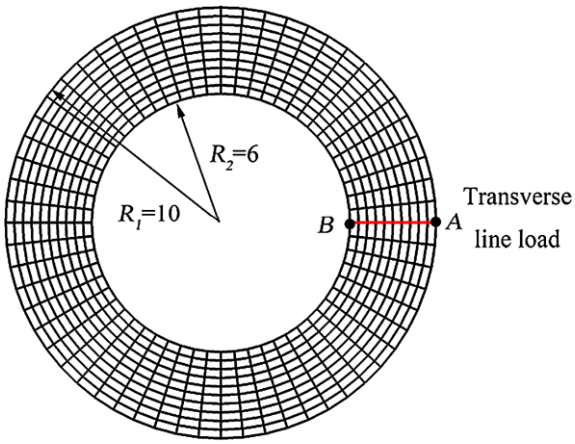

Fig. 4 Clamped slit annular plate (60 × 10 mesh)

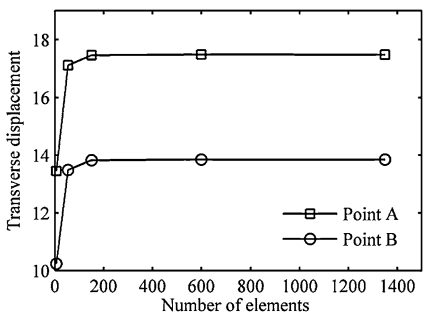

Fig. 5 Transverse displacements of points A and B under load $q = 0.8$ versus number of elements for the clamped slit annular plate

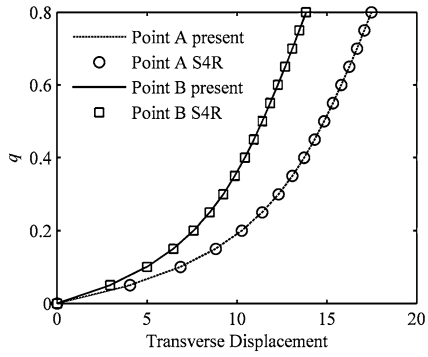

Fig. 6 Transverse displacements of points A and B versus load for the clamped slit annular plate (90 × 15 mesh)

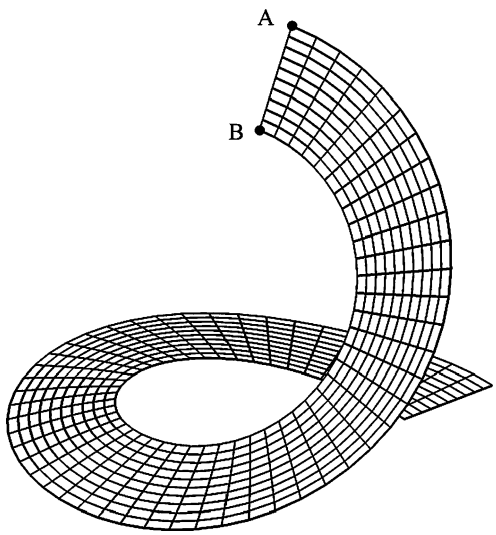

Fig. 7 Deformed configuration of the clamped slit annular plate under load $q = 0.8$ (60 × 10 mesh)

[22, 24], which is not modeled by ANCF element before because of its initially curved shape. The whole hemispherical shell with 18° hole has radius of 10 and thickness of 0.04, and only one quarter of the shell is modeled owing to its symmetry, shown in Fig. 8. The Young's modulus and Poisson's ratio are 6.825×10^7 and 0.3, respectively. For convergence test shown in Fig. 9, the displacements of points A and B (Fig. 8) under $P = 400$ are plotted as a function of the number of elements, 1 (latitude direction) × 1 (longitude direction), 8 × 6, 15 × 12, 24 × 18 and 30 × 24. The deflection curves of the two measuring points versus applied force are shown in Fig. 10, where the results of the proposed element are in good agree-

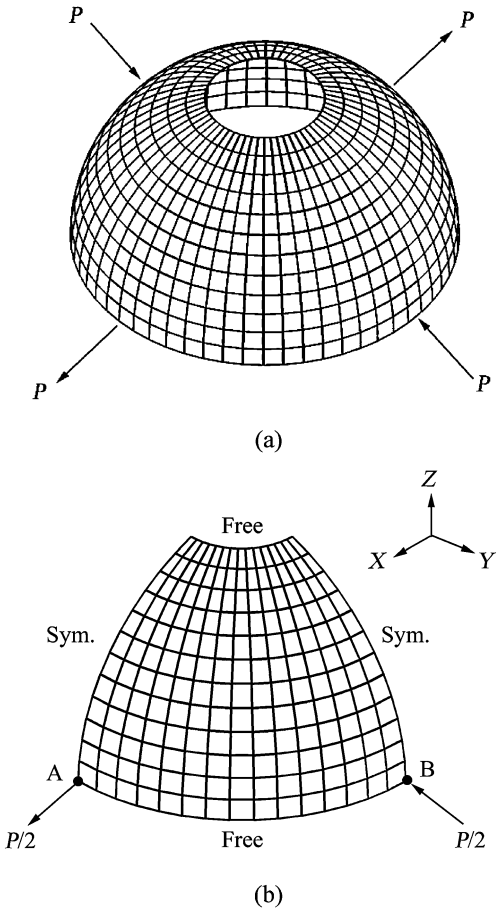

Fig. 8 (**a**) Hemispherical shell with 18° hole, (**b**) one quarter finite-element model (15 × 12 mesh)

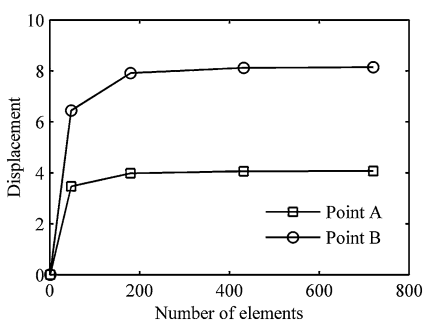

Fig. 9 Displacements (absolute value) of points A and B under $P = 400$ versus number of elements for the hemispherical shell with 18° hole

ment with those of the S4R element in ABAQUS. The deformed configuration at $P = 400$ are visualized in Fig. 11.

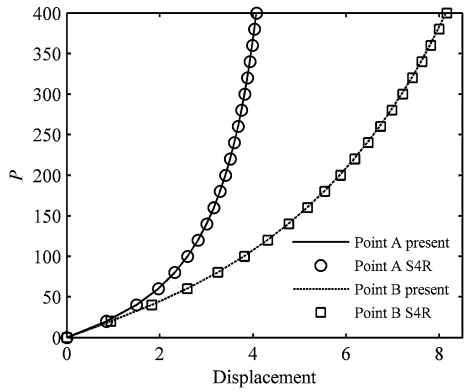

Fig. 10 Displacements (absolute value) of points A and B versus load for the hemispherical shell with 18° hole (30 × 24 mesh)

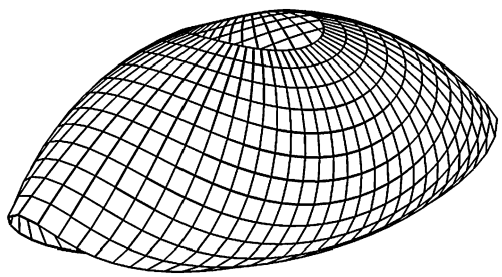

Fig. 11 Deformed configuration of the hemispherical shell with 18° hole when P is 400 (15 × 12 mesh)

4.4 Hemispherical shell without hole

In this subsection, a full hemispherical shell without the hole is calculated. The mesh lines are not smooth when only quadrilateral elements are used, and obvious on-surface slope discontinuities are present, as shown in Fig. 12. This case is intended to examine the validity of the formulation given in Sects. 2 and 3. The geometry and material parameters as well as the load are the same as those of the previous subsection. In Fig. 13, the displacements of points A and B (Fig. 12) under $P = 400$ are plotted as a function of the number of elements (1 × 1 × 3, 4 × 4 × 3, 8 × 8 × 3, 12 × 12 × 3, 16 × 16 × 3). The deflection curves of the two measuring points versus applied force are compared with the results of S4R element of ABAQUS in Fig. 14, where good agreements are observed. The deformed configuration at $P = 400$ are plotted in Fig. 15.

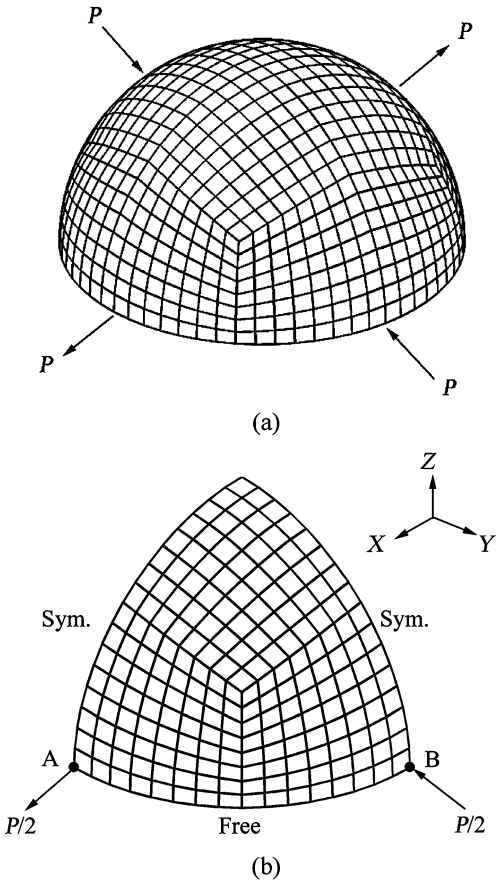

Fig. 12 (**a**) Full hemispherical shell, (**b**) one quarter finite-element model (8 × 8 × 3 mesh)

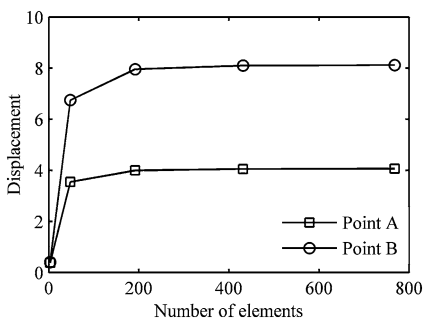

Fig. 13 Displacements (absolute value) of points A and B under $P = 400$ versus number of elements for the hemispherical shell without hole

4.5 Octant spherical shell pendulum

In this case, a free falling of an octant spherical shell pendulum is simulated to examine the capacity for modeling dynamics with the proposed curved shell element, where the on-surface slope discontinuities are included. The Young modulus of the material is 6.825×10^7, material density is 7810, and Poisson ratio is 0.3. The geometry properties are radius of 0.5 and thickness of 0.01. The three corners of the shell are initially placed on the horizontal plane with the concave side upward. One corner point is restrained to ground via a spherical joint, in which all the translation displacements of the node are fixed and the rotations are free, as shown in Fig. 16.

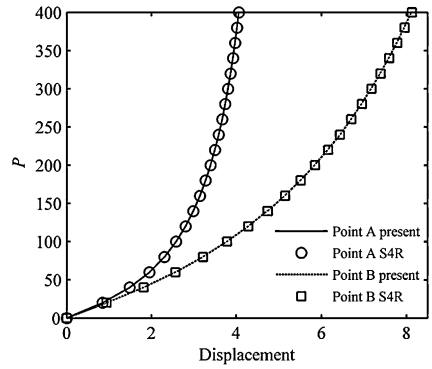

Fig. 14 Displacements (absolute value) of points A and B versus load for the hemispherical shell without hole (16 × 16 × 3 mesh)

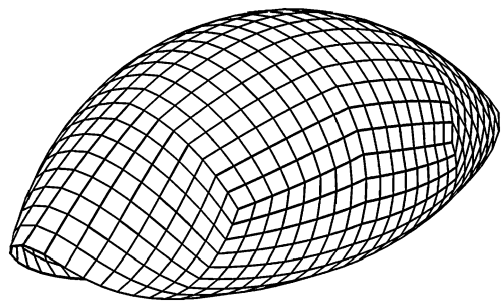

Fig. 15 Deformed configuration of the hemispherical shell without hole when P is 400 (8 × 8 × 3 mesh)

The Z-coordinate of point A on the pendulum (Fig. 16) is graphed as a function of time in Fig. 17 within the simulation time of 1 second, where cases of four mesh densities (1 × 1 × 3, 4 × 4 × 3, 8 × 8 × 3, 16 × 16 × 3) are examined. It can be seen from Fig. 17 that considerable convergent result is obtained up to the 8 × 8 × 3 mesh. To ensure the correctness of the simulated physics, the global energy balance of the system is monitored, and graphed in Fig. 18 with respect to the time, where T, V and U are kinetic energy, deformation energy and potential energy of the octant

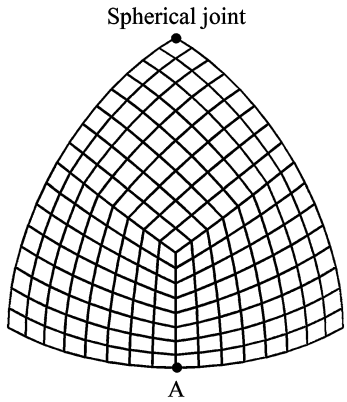

Fig. 16 Octant spherical shell pendulum (8 × 8 × 3 mesh)

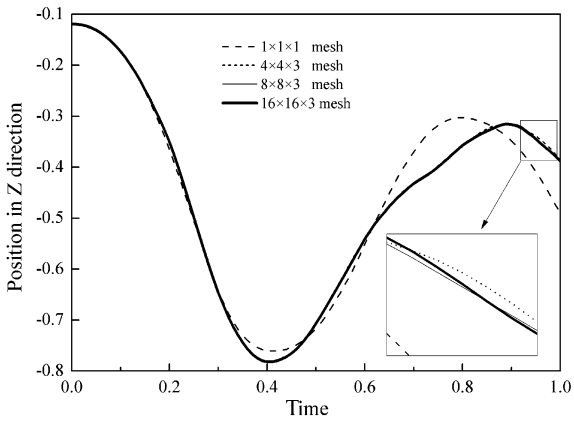

Fig. 17 The motion of point A in Z-direction of the octant spherical shell pendulum with different mesh densities

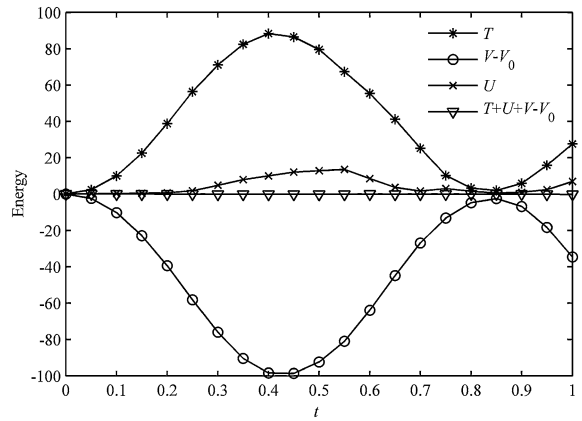

Fig. 18 Energy balance of the free falling octant spherical shell pendulum (16 × 16 × 3 mesh)

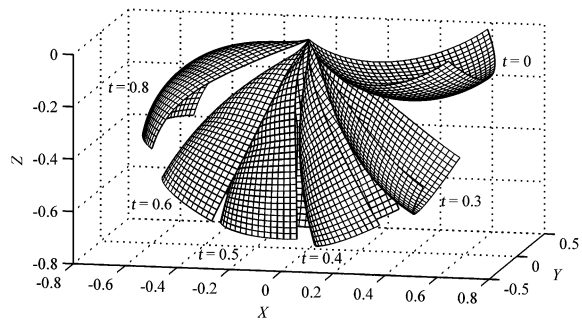

Fig. 19 Dynamic deformed configurations of the octant spherical shell pendulum (16 × 16 × 3 mesh)

spherical shell, respectively. Since the falling pendulum is a conservative system, the sum of the energy should conserve all the time. From Fig. 18, the conservation of the system energy is observed at each time point, where a 16 × 16 × 3 mesh is used for the calculation. Finally, Fig. 19 shows several snapshots of the deformed configuration with 16 × 16 × 3 mesh.

5 Conclusions

In this paper, a curved gradient deficient shell element is proposed based on the Green–Lagrange strain measured with respect to the curvilinear coordinate system characterizing the reference configuration. The element formulation and its simplified form of thin curved gradient deficient shell element are derived, and the initial strain due to the initial curved configuration is naturally eliminated. The degenerated 2D version is identical with the 2D curved beam element in the previous work. In the discretization of a general curved thin structure regular mesh can seldom be obtained, therefore on-surface slope discontinuities usually occur even if the surface is smooth. A constant on-surface transformation is provided for the modeling of curved surface with irregular mesh, hence the feature of constant mass matrix of ANCF is maintained. The performance of the developed element is verified by numerical examples.

Acknowledgements This work was supported in part by National Natural Science Foundation of China under Grant Nos. 10972036, 10832002, 11221202, 11202025 and 11290151.

References

1. Shabana, A.A.: An absolute nodal coordinate formulation for the large rotation and deformation analysis of flexible

bodies. Technical report #MBS96-1-UIC, University of Illinois at Chicago (1996)
2. Schiehlen, W.: Computational dynamics: theory and applications of multibody systems. Eur. J. Mech. A, Solids **25**, 566–594 (2006)
3. Schiehlen, W.: Research trends in multibody system dynamics. Multibody Syst. Dyn. **18**, 3–13 (2007)
4. Sugiyama, H., Shabana, A.A.: Application of plasticity theory and absolute nodal coordinate formulation to flexible multibody system dynamics. J. Mech. Des. **126**, 478–487 (2004)
5. Sugiyama, H., Shabana, A.A.: On the use of implicit integration methods and the absolute nodal coordinate formulation in the analysis of elasto-plastic deformation problems. Nonlinear Dyn. **37**, 245–270 (2004)
6. Omar, M.A., Shabana, A.A.: A two-dimensional shear deformable beam for large rotation and deformation problems. J. Sound Vib. **243**, 565–576 (2001)
7. Shabana, A.A., Yakoub, R.Y.: Three dimensional absolute nodal coordinate formulation for beam elements: theory. J. Mech. Des. **123**, 606–613 (2001)
8. Sugiyama, H., Suda, Y.: A curved beam element in the analysis of flexible multi-body systems using the absolute nodal coordinates. Proc. Inst. Mech. Eng., Proc., Part K, J. Multi-Body Dyn. **221**, 219–231 (2007)
9. Mikkola, A.M., Shabana, A.A.: A non-incremental finite element procedure for the analysis of large deformation of plates and shells in mechanical system applications. Multibody Syst. Dyn. **9**, 283–309 (2003)
10. Garcia-Vallejo, D., Mikkola, A.M., Escalona, J.L.: A new locking-free shear deformable finite element based on absolute nodal coordinates. Nonlinear Dyn. **50**, 249–264 (2007)
11. Berzeri, M., Shabana, A.A.: Development of simple models for the elastic forces in the absolute nodal co-ordinate formulation. J. Sound Vib. **235**, 539–565 (2000)
12. Gerstmayr, J., Irschik, H.: On the correct representation of bending and axial deformation in the absolute nodal coordinate formulation with an elastic line approach. J. Sound Vib. **318**, 461–487 (2008)
13. Gerstmayr, J., Shabana, A.A.: Analysis of thin beams and cables using the absolute nodal co-ordinate formulation. Nonlinear Dyn. **45**, 109–130 (2006)
14. Dmitrochenko, O.N., Pogorelov, D.YU.: Generalization of plate finite elements for absolute nodal coordinate formulation. Multibody Syst. Dyn. **10**, 17–43 (2003)
15. Dufva, K., Shabana, A.A.: Analysis of thin plate structures using the absolute nodal coordinate formulation. Proc. Inst. Mech. Eng., Proc., Part K, J. Multi-Body Dyn. **219**, 345–355 (2005)
16. Sugiyama, H., Koyama, H., Yamashita, H.: Gradient deficient curved beam element using the absolute nodal coordinate formulation. J. Comput. Nonlinear Dyn. **5**, 021001 (2010)
17. Liu, C., Tian, Q., Hu, H.Y.: New spatial gradient deficient curved thin beam and plate elements of the absolute nodal coordinate formulation. Nonlinear Dyn. **70**, 1903–1918 (2012)
18. Shabana, A.A., Mikkola, A.M.: Use of the finite element absolute nodal coordinate formulation in modeling slope discontinuity. J. Mech. Des. **125**, 342–350 (2003)
19. Shabana, A.A., Maqueda, L.G.: Slope discontinuities in the finite element absolute nodal coordinate formulation: gradient deficient elements. Multibody Syst. Dyn. **20**, 239–249 (2008)
20. Shabana, A.A.: General method for modeling slope discontinuities and T-sections using ANCF gradient deficient finite elements. J. Comput. Nonlinear Dyn. **6**, 024502 (2011)
21. Huang, K.Z.: Nonlinear Continuum Mechanics. Tsinghua University Press, Beijing (1989) (in Chinese)
22. Kulikov, G.M., Plotnikova, S.V.: Non-linear exact geometry 12-node solid-shell element with three translational degrees of freedom per node. Int. J. Numer. Methods Eng. **88**, 1363–1389 (2011)
23. Arciniega, R.A., Reddy, J.N.: Tensor-based finite element formulation for geometrically nonlinear analysis of shell structures. Comput. Methods Appl. Mech. Eng. **196**, 1048–1073 (2007)
24. Schwarze, M., Reese, S.: A reduced integration solid-shell finite element based on the EAS and the ANS concept-geometrically linear problems. Int. J. Numer. Methods Eng. **80**, 1322–1355 (2009)
25. Sanborn, G.G., Choi, J., Choi, J.H.: Curve-induced distortion of polynomial space curves, flat-mapped extension modeling, and their impact on ANCF thin plate finite elements. Multibody Syst. Dyn. **26**, 191–211 (2011)
26. Borisenko, A.I., Tarapov, I.E.: Vector and Tensor Analysis with Applications. Dover Publications, New York (1979)